Applied Thermal Engineering 233 (2023) 121146

Contents lists available at ScienceDirect

Applied Thermal Engineering

journal homepage: www.elsevier.com/locate/apthermeng

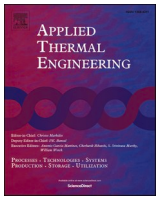

Research Paper

A novel method to measure the energy efficiency and performance of an auto-cascade refrigeration cycle

Rodrigo Llopis *, Manel Martínez-Ángeles, Marc García-Valero

Thermal Engineering Group, Mechanical Engineering and Construction Department, Jaume I University, Spain

ARTICLE INFO

Keywords:
Auto-cascade
Measurement
COP
Ultra-low temperature
Energy efficiency

ABSTRACT

Auto-cascade refrigeration systems are the most used cycles to maintain spaces at ultra-low temperature conditions (-80 to −60 °C). The interest in these systems has risen due to the need to maintain and distribute COVID-19 vaccines. However, there is a lack of experimental validation of the theoretical models that are used to analyse and optimize them. In this work, a novel method to calculate the thermodynamic performance, circulating compositions, and energy efficiency of an auto-cascade refrigeration system is presented. The method is based on the measurements of an experimental auto-cascade plant at temperatures from −83.0 to −59.9 °C. The results of the study showed that the proposed calculation method was able to accurately predict the thermodynamic performance, circulating compositions and energy efficiency of an auto-cascade system. The uncertainty of the predictions was found to be below 1% for circulating compositions and 5.2% for the cooling capacity and COP.

1. Introduction

Refrigeration is recognised as a technology necessary for the welfare of humanity, but the COVID-19 pandemic has raised its importance, as most of the vaccines need to be distributed and stored in ultra-low temperature conditions. According to the International Institute of Refrigeration, more than 7 billion COVID-19 vaccines were ordered at the end of 2020, with storage temperatures ranging from −90 to 8 °C [1]. In addition, the pandemic highlighted the shortage of ultra-low temperature refrigeration systems worldwide, and it is expected their need will grow exponentially, especially in the end-user spaces such as hospitals, pharmacies, or vaccination points. For these uses, the most used refrigeration architecture corresponds to the auto-cascade (AC) refrigeration system (Fig. 1), which is a cycle working with a pair of fluids with very different normal boiling points that are fractionated inside the cycle, performing like a cascade cycle but driven by only one compressor, as discussed by Mota-Babiloni et al. [2].

The first AC commercial systems for ultra-low temperature (around −80 °C) operated with the fluids R-134a and R-23, where R-134a had the highest (-26.36 °C) and R-23 had the lowest (-82.24 °C) normal boiling points. However, after the approval of the F-Gas Regulation [3], which banned the use of fluids with high GWP, the use of R-23 decreased (although its use is still permitted) and new systems are built with the pair isobutane (R-600a) as the least volatile component (NBP = -12.08 °C) and ethylene R-1150 (NBP = -103.99 °C) as the most volatile component. With this pair, the AC system (Fig. 1) is able to produce two currents of refrigerant in the phase separator (PHS): The fluid that comes out from the bottom of the PHS contains a higher proportion of the least volatile component (R-600a) and is used internally in the cycle. The fluid released from the top of the PHS is enriched in the most volatile component (R-1150) and is condensed and subcooled in the cascade heat exchanger (CHX). This current, after lamination, reaches very low temperatures at the inlet of the refrigerated space, providing the cooling effect.

In the last 10 years, there has been a rising scientific interest in this cycle, initially driven by the avoidance of R-23 and later due to the COVID pandemic. From a theoretical approach, Wang et al. [4] focused on the use of mixtures of ethane (R-170/R-290, R-170/R-600 R-170/R-600a) for application up to −60 °C in a two-stage AC system with two separators, while He et al. [5] considered a simple AC system. Yan et al. [6,7] considered mixtures with propane (R-290/R-600, R-290/R-600a) for a dual temperature refrigeration system based on a single-AC system for applications at −30 °C. Rodríguez-Jara et al. [8], Liu et al. [9,10], Li et al. [11] and He et al. [5] used different AC layouts and considered the mixture R-600a/R-1150 for temperatures up to −80 °C, and recently extended the investigation to the use of other zeotropic refrigerant mixtures [12]. Finally, Chen et al. [13] released a 4E analysis about the use of a simple AC system in relation to advanced AC systems including two-phase separators and ejectors, highlighting the opportunities of

* Corresponding author.
E-mail address: rllopis@uji.es (R. Llopis).

https://doi.org/10.1016/j.applthermaleng.2023.121146
Received 5 February 2023; Received in revised form 3 July 2023; Accepted 8 July 2023
Available online 10 July 2023

Nomenclature

AC	auto-cascade refrigeration system
CHX	cascade heat exchanger
COP	coefficient of performance
h	specific enthalpy, $J \cdot kg^{-1}$
I	calculated uncertainty
IHX	internal heat exchanger or recuperator
$\dot{m}$	refrigerant mass flow rate, $kg \cdot s^{-1}$
NBP	normal boiling point, ºC
p	absolute pressure, bar
PHS	phase separator
P_C	compressor power consumption, W
$\dot{Q}$	heat transfer rate, W
t	temperature, °C
x	vapor quality
X	represents a parameter
Z	mass percentage composition of R-1150
$Z_{l,e}$	equilibrium liquid mass percentage composition
$Z_{v,e}$	equilibrium vapour mass percentage composition

Greek symbols

ε	sensor measurement error
ρ	density, $kg \cdot m^{-3}$

Subscripts

chx	cascade heat exchanger
dis	compressor discharge
env	environment
exp	expansion
k	condenser
l	refers to the refrigerant composition of fractionated liquid
mix	mixing point
o	evaporator, outlet, value without uncertainty
rs	refrigerated space
t	refers to the refrigerant composition through the compressor
sub	subcooled
suc	compressor suction
v	refers to the refrigerant composition of fractionated vapor

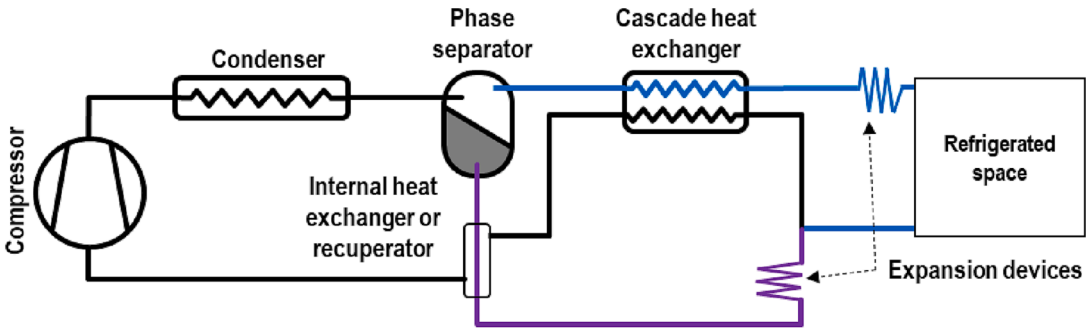

Fig. 1. Schematic representation of an AC refrigeration cycle.

COP enhancement using new but more complex layouts. The main objective of these theoretical works was to optimize and quantify the energy performance of the different solutions and to optimize the mixture compositions for the required temperature level. However, due to the lack of experimental studies of these systems, most of the authors had to consider assumptions which were not verified experimentally. Most used an expression to estimate the compressor efficiency coming from an old study of an R-22 compressor, all considered that the circulating compositions in the cycle coincided with the charging ones; and considered complete phase separation in the vessels. These works constitute the best information for the design and understanding of these systems, but an experimental verification of the assumptions is needed to check the consistency of the results.

Experimental investigations of AC refrigeration systems are scarce and main only focus on the achieved ultra-low temperatures and the pull-down processes. Aprea and Maiorino [14] were able to build a system for temperatures up to −150 °C using with a non-revealed mixture of 7 components (R-507, R-245fa, R-116, R-23, R-14, R-744, R-290) using an interesting two-stage AC system. They focused their analysis on the pull-down characteristics, the control during the start-up to avoid very high discharge pressures, and on the achieved temperature. Obviously, the complexity of the system and the unknown circulating composition prevented the calculation of a COP value. Du et al. [15] developed a single-stage AC plant working with R-23 and R-134a, reaching −66.4 °C. They tried to quantify the COP using simulation, but they obtained large differences between the predicted experimental data and those calculated from simulation. Zhang et al. [16] built a CO_2/R-290 AC and also tried to validate an experimental COP with simulation, but, as with previous authors, there was a large deviation. Finally, the most recent experimental results were published by Bai et al. [17,18] using a single-stage ejector enhanced AC with R-134a/R-23. They pointed out that the circulating compositions would differ from the charging ones according to the experimental behaviour of the plant and evaluated the cooling capacity and COP of the system by calculating the heat transfer to the refrigerated space and the energy input from an electrical heater. Perhaps, this is the first time that a reliable COP value of an AC system is published, but it was obtained from its interaction with the surroundings and not through the refrigeration cycle. A similar procedure was used to measure the COP and cooling capacity by Qin et al. [19], but in this case they operated with a Linde-Hampson cycle coupled thermally with an AC cycle for temperatures near −150 °C. They provided COP values, but they did not report their uncertainty.

Although the AC systems work and are commercially available, up to this moment their energy efficiency (COP) and behaviour have not been measured experimentally, mainly because this system involves to many unknown issues. To the knowledge of the authors, this work presents for the first time a measurement system and a calculation method that allows for the calculation of all the thermodynamic states of the fluids inside the cycle, the circulating compositions and the COP and cooling capacity with an acceptable uncertainty. The work describes the test rig, measurement system, experimental tests, and proposes a calculation method with its validation. The objective is to share the method to boost

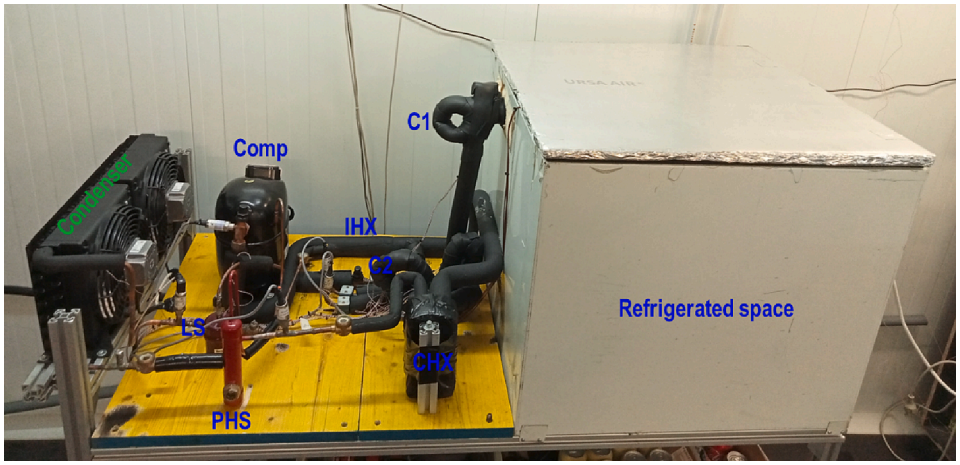

Fig. 2. Photography of the experimental test rig.

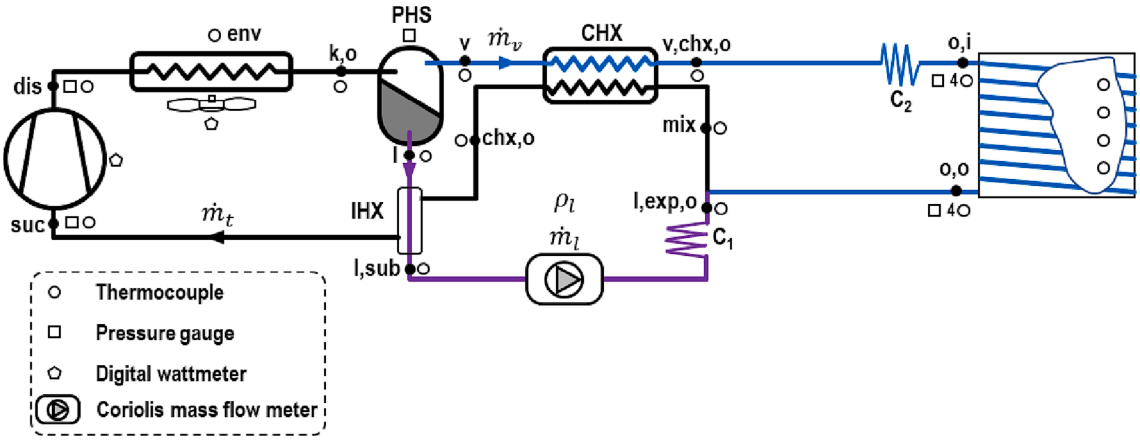

Fig. 3. Experimental test rig scheme, sensors allocation and reference points.

the research of ultra-low temperature systems. It needs to be mentioned that the objective of the experimental tests and this manuscript was to develop the measurement method and not achieving its energy optimization, which will be dealt with soon.

2. Experimental system and test

2.1. Test rig

The plant (Fig. 2) corresponds to a single-stage AC refrigeration system, the scheme of which is detailed in Fig. 3. This system is designed to provide very low temperatures by fractionating a mixture of two refrigerants with distant normal boiling points in the phase separator (PHS). It is driven by an R-404A semihermetic compressor of 34.38 cm^3 displacement and 1.12 kW of nominal power. It incorporates a mini channel air cooled condenser, a brazed-plate cascade heat exchanger (CHX) (0.216 m^2), and a double pipe (0.03 m^2) internal heat exchanger (IHX) or recuperator heat exchanger. The PHS is placed at the exit of the condenser and divides the refrigerant into two currents: the vapour flows to the CHX and the liquid is expanded using a capillary tube (C_2, 2.5 m, 0.8 mm inner diameter) and sent to the CHX to condensate the vapour. Subcooled vapour is expanded using a second capillary (C_1, 3.5 m, 0.8 mm inner diameter) and sent to the evaporator of the refrigerated space This space has a storage dimension of 0.5 × 0.5 × 0.5 m and incorporates 10 m of 3/8 in. tube welded on the plate of the container, acting as evaporator. The space is insulated with 120 mm width using high density expanded polyurethane and the rest of the system with 40 mm width Armaflex insulation. In addition, a high-efficiency oil separator is placed at the compressor discharge.

The thermodynamic cycle (see Fig. 3 and Fig. 7 for better understanding) is as follows: the compressor compresses the superheated vapour (*point suc*) from the low pressure to high pressure (*point dis*). The refrigerant is then partially condensed in the condenser and sent to the PHS, where the refrigerant with the initial mass composition Z_t is fractionated and divided into two streams. From the top of the PHS, saturated vapour with composition Z_v (*point v*) is extracted and sent to the CHX. This situation is verified experimentally through an eyehole place on the vapour line as seen in Fig. 2. In the CHX, it is fully condensed and subcooled, then expanded using the capillary C_2 and sent to the evaporator. At this point (*point o,i*) the fluid reaches its lowest temperature. In the evaporator, the fluid absorbs energy from the refrigerated space and leaves the evaporator in a two-phase state at a temperature very close to that of the refrigerated space. From the bottom of the PHS, a two-phase state fluid with composition Z_l is extracted (*point l*). It is subcooled in the IHX and then expanded using the capillary C_1 to low pressure. The two streams then merge (*point mix*), reaching the initial composition Z_t, and are used to condensate and subcool the refrigerant in the CHX. At the exit (*point chx,o*), the fluid is still in two-phase state and it is completely evaporated in the IHX.

This system has only two pressure levels, but three currents with different compositions. We denote the mass composition of the fluid through the compressor as Z_t (black line Fig. 3), the mass composition of the saturated vapour leaving the PHS as Z_v (blue line Fig. 3), and the mass composition of the two-phase fluid leaving the PHS from the

Table 1
Measurement devices, range, and uncertainties.

Measurement	Variables	Device	Range	Uncertainty
Liquid density	ρ_l	Coriolis mass flow meter	300 to 700 kg·m^{-3}	±0.2% of measurement
Pressure	p_{dis}, $\boldsymbol{p_{phs}}$	Pressure gauge	0 to 31 bar_{abs}	±1% of measurement
Pressure	$p_{o,in}$, $\boldsymbol{p_{o,out}}$, $\boldsymbol{p_{suc}}$	Pressure gauge	0 to 9 bar_{abs}	±1% of measurement
Temperature	$\boldsymbol{t_{suc}}$, t_{dis}, $\boldsymbol{t_{k,o}}$, t_v, $\boldsymbol{t_{v,chx,o}}$, t_l, $\boldsymbol{t_{l,sub}}$, $t_{l,\exp,o}$, t_{mix}, $t_{chx,o}$, t_{env}	Surface T-type thermocouple	−150 to 200 °C	0.5 K
Temperature	$t_{o,i}$, $\boldsymbol{t_{o,o}}$	4 surface T-type thermocouple	−150 to 200 °C	0.25 K
Temperature refrigerated space	$t_{r,1}$, …, $t_{r,4}$	T-type thermocouple inside 25 g brass cylinder	−150 to 200 °C	0.5 K
Liquid mass flow rate	$\dot{m}_l$	Coriolis mass flow meter	0 to 12 kg·h^{-1}	±0.25% of measurement
Power consumption	P_c, P_{fan}	Digital wattmeter	0 to 4 kW	±0.5% of measurement

bottom as Z_l (purple line Fig. 3). The fractionation in the PHS creates two currents of fluids with very different characteristics. The vapour with composition Z_v has high proportion of the most volatile component, which allows for reaching very low temperatures in the evaporator. The liquid with composition Z_l contains a higher proportion of the less volatile component, which is used to condensate and subcool the other current, but does not provide cooling effect in the system.

The plant is fully instrumented, with the sensors listed in Table 1 and the positions detailed in Fig. 3. It incorporates 5 pressure gauges, a Coriolis mass flow meter, two digital wattmeters and 23 T-type thermocouples. Temperature at the inlet and outlet of the evaporator of the refrigerated space is measured averaging the measurement of four thermocouples around the tube surface (top of the tube, bottom, left and right) to reduce the uncertainty of the method. Temperature of the refrigerated space is considered as the average temperature of four T-type thermocouples inserted inside 25 g brass cylinders. They are located at 5, 10, 15 and 20 cm from the bottom of the space. Brass cylinders are used to reduce the measurement noise and to reduce quick compressor starts. All the information is gathered by a cRIO-9074 daq system and handled using LabView. Subsection 2.3 provides a detailed analysis of the measurement system.

2.2. Reference test

Characterization of the AC is based on an experiment lasting approximately 80 h (Fig. 4 and Fig. 5). The plant was charged with 340 g of a mixture of isobutane/ethylene (R-600a/R-1150) with a mass composition of 70/30% (238 ± 1 g of R-600a and 102 ± 1 g of R-1150). It was then placed in a climatic chamber at a temperature of 25.0 ± 0.5 °C and underwent a pull-down up to −82.0 °C (initial cooling process). It then operated continuously for three hours at the lowest achievable temperature (-83.0 °C) and was run around 14 h at different set points using compressor ON-OFF control regulation. Fig. 4 details the evolution of the mean temperature of the refrigerated space (t_{rs}) and the environment temperature at the air inlet of the condenser (t_{env}); and Fig. 5 the evolution of the two cycle pressures, compressor's discharge (p_{dis}) and suction (p_{suc}). Characterization in quasi-steady-state conditions was done averaging the measurements during 20 s for three points at each temperature of the refrigerated space, with the moment before the compressor switch-off being selected. Considered points are highlighted with a black dot in Fig. 5. All the experimental data that supports this study are detailed in Appendix 2.

As shown in Fig. 5, the suction pressure when the compressor is ON remains practically constant throughout all the test (1.30 ± 0.13 bar). It is the usual behaviour in systems working with capillary tubes used as expansion devices. However, the discharge pressure reaches a maximum during the start-up of the compressor (24.25 bar) and, as the refrigerated space reduces its temperature, it decreases until the compressor stops. This behaviour is observed throughout all the test, but the final pressure has a clear dependence on the temperature of the refrigerated space. Fig. 6 depicts the pressures of the selected points at the different temperatures of the refrigerated space. It can be clearly observed that, although the environment temperature remains constant, there is a dependence, ranging from 12.05 bar at −83.0 °C to 15.31 at −59.5 °C. This phenomenon was also observed by Aprea and Maiorino [14] in a two-stage AC and by Du et al. [15] in a single stage AC. However, only Du et al. [15] suggested a reason to explain it, saying that, as the evaporator temperature decreases, the concentration of the most volatile component in the liquid current increased while part of the it is retained in the evaporator. They did not report any justification for this affirmation. Finally, Bai et al. [17,20] using a single-stage ejector

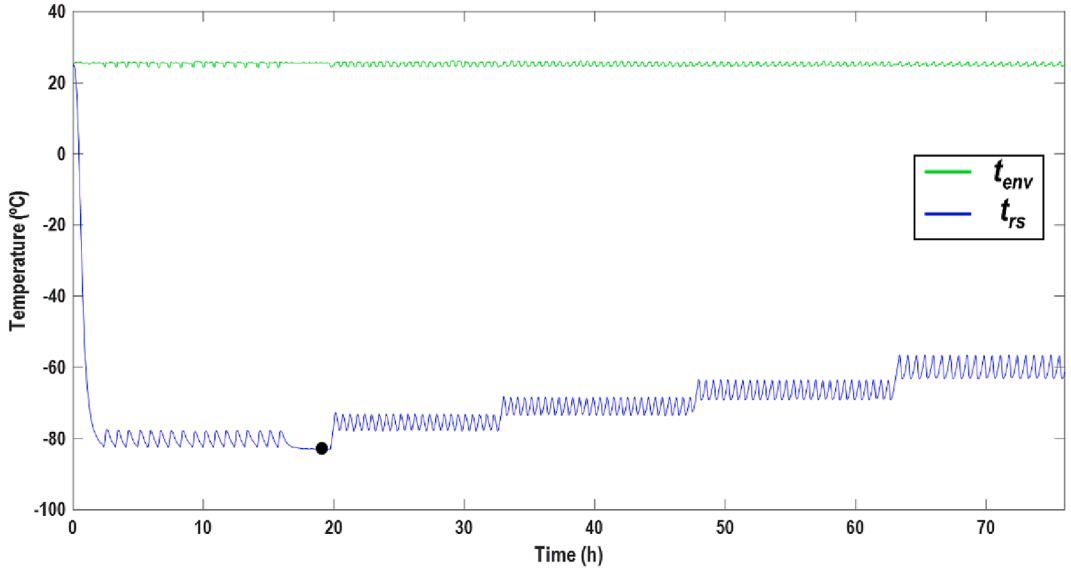

Fig. 4. Pull-down and cycling temperature tests of test rig.

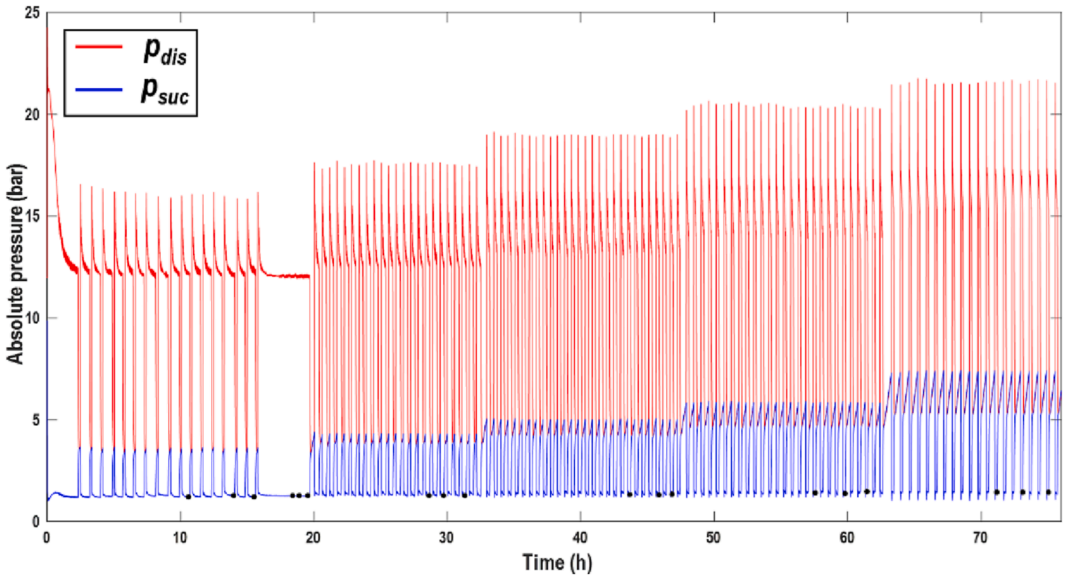

Fig. 5. Discharge and suction pressure during the test.

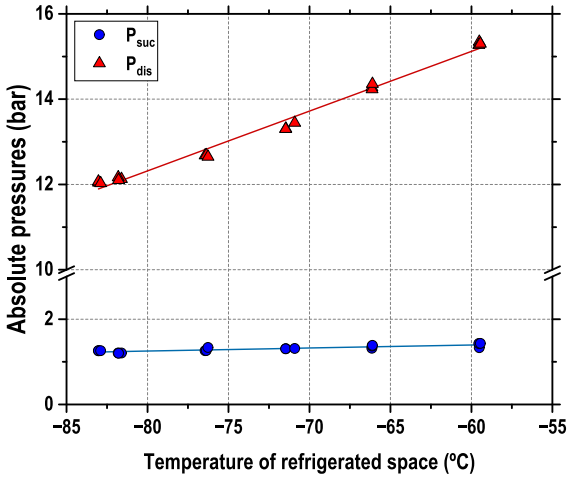

Fig. 6. Steady-state pressures vs. average temperature of the refrigerated space.

enhanced AC suggested that the circulating concentrations may differ from the charging ones, but they did not report more information in their work.

Considering the results of Fig. 6, we can affirm that there is a reason for the high-pressure dependence, but no complete explanation has been given at this time. It could be associated with a change in the mass composition of the circulating refrigerant or to an accumulation of the refrigerant in the evaporator. These affirmations are in agreement with the results of Sreenivas et al. [21] for a Joule-Thomson refrigeration cycle and with those of Chen et al. [22] for a dual temperature refrigeration system. However, the real behaviour of an AC system has not been fully explored yet, since a methodology to evaluate the circulating concentration of the fluid and the energy performance has not been developed yet.

2.3. Measurement special features and considerations

Up to now, to the knowledge of the authors, the calculation of the thermodynamic states of the cycle, the energy parameters (cooling capacity and COP) and their uncertainties of an AC refrigeration system has not yet been achieved, due to the system's several challenging special features:

- The composition of the circulating fluid is different from the charging one, and it is modified at different temperatures of the refrigerated space.
- Most of the thermodynamic states are in two-phase condition (see Fig. 7). In a blend of two components with distant normal boiling points, there is a large temperature difference during the phase change process at constant pressure, so uncertainty in temperature

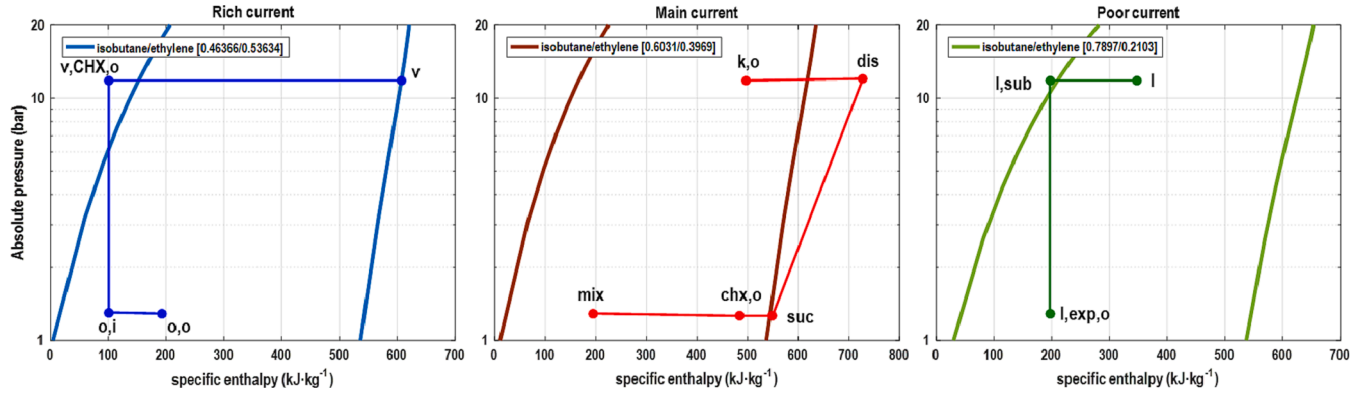

Fig. 7. Pressure-enthalpy diagrams of the three currents with different composition at reference point of Fig. 4.

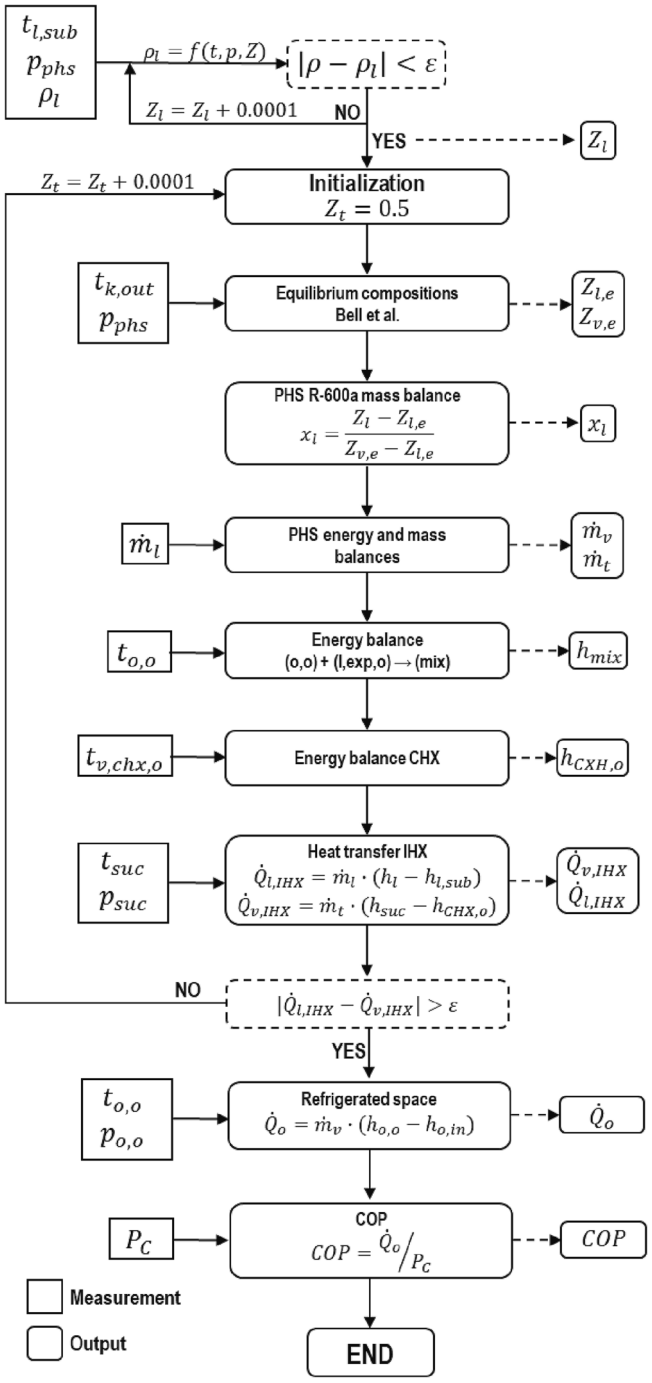

Fig. 8. Energy performance calculation method.

measurement implies a large uncertainty in the specific enthalpy calculation.

- The cycle involves three refrigerant flows ($\dot{m}_t$, $\dot{m}_v$ and $\dot{m}_l$).
- In most of cases, the refrigerant at the exit of the PHS is not in liquid saturated condition, but rather in a two-phase state.

We propose a novel method that allows for the calculation of circulating compositions, thermodynamic states, and energy parameters with an acceptable degree of uncertainty (described in Section 3) based on the following considerations:

- Measurement of liquid density by a Coriolis mass flow meter with high precision (ε_ρ less than 0.2%) is the key parameter to determine the mass composition of the liquid current (Z_l). The Coriolis is strategically placed after the IHX to guarantee a large subcooling degree, avoiding bubble formation during the measurement. No other position of a Coriolis is recommended, since in vapour phase it introduces a large pressure drop, it does not measure into two phase condition, and it cannot operate at temperatures below −50 °C (*point v,chx,o*).
- Thermodynamic equilibrium is assumed in the PHS, CHX, and IHX. The heat exchangers are isolated, therefore, the energy transfer from both fluids currents is equal. In equilibrium, the PHS satisfies the energy balance and the mass balance of each component separately, since there is no chemical interaction between the fluids.
- Refprop v.10 [23], which is the database used to calculate the thermodynamic properties of the fluids, includes the mixture model for the binary mixture ethylene (R-1150) and isobutane (R-600a).
- The plant contains a high-efficiency lubricant separator, so the effects of the lubricant oil on the thermophysical properties are neglected.

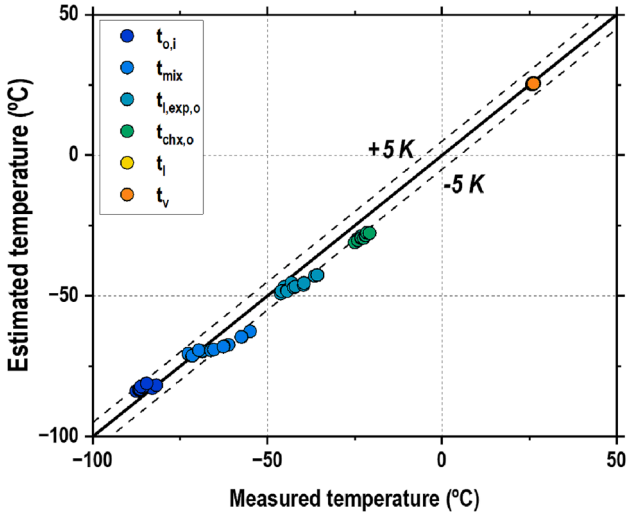

Fig. 9. Validation of temperature check points.

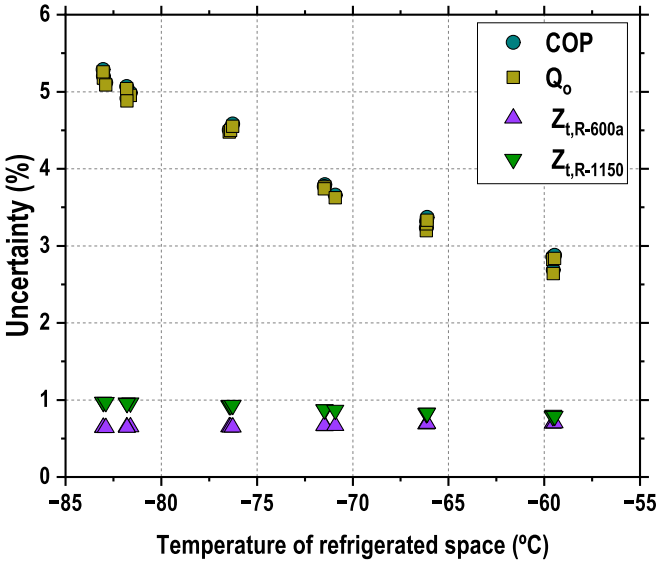

Fig. 10. Percentage uncertainty vs. temperature of refrigerated space.

3. Method and validation

This section describes the method for calculating energy

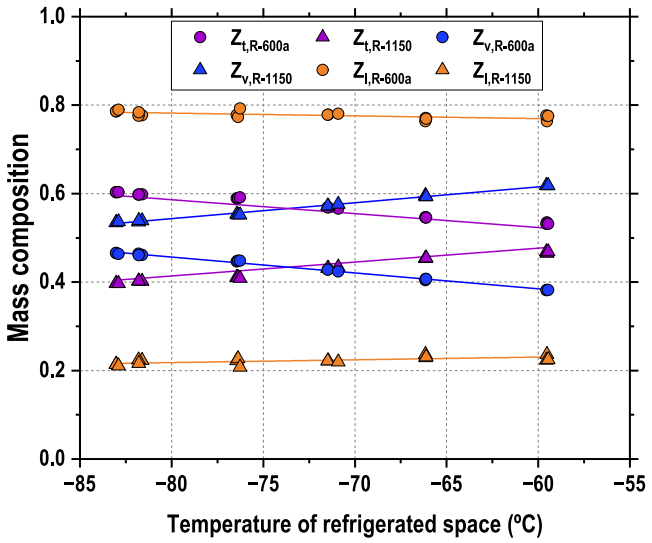

Fig. 11. Mass compositions of the three currents vs. temperature of refrigerated space.

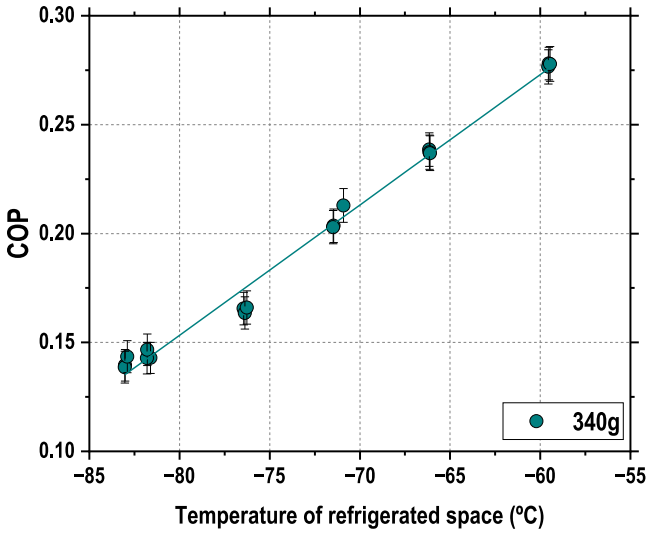

Fig. 12. COP vs. temperature of refrigerated space.

performance, its validation, and the calculation of the associated uncertainty.

3.1. Energy performance calculation method

Proposed method, based on the measurement of eleven sensors and the considerations detailed in Subsection 2.3, is summarized by the iterative calculation scheme of Fig. 8. This method allows for the calculation of the circulating compositions, the specific enthalpies of the fluids, and the energy parameters of the cycle.

The method determines the liquid composition (Z_l) using temperature, pressure and liquid density at the point '*l,sub*' with Eq. (A. 1). Starting from an initial value, the concentration of the first component is increased until the calculated density matches with the measurement of the Coriolis. Next, the method assumes an initial value of the mass composition of the first component of the fluid circulating through the compressor (Z_t). For this composition, the method estimates the fractionated equilibrium composition in the PHS ($Z_{l,e}, Z_{v,e}$) using its inlet pressure and temperature with Bell et al. correlations with Eq. (A. 2) [24] and calculates the vapour title at the bottom of the PHS (x_l, point

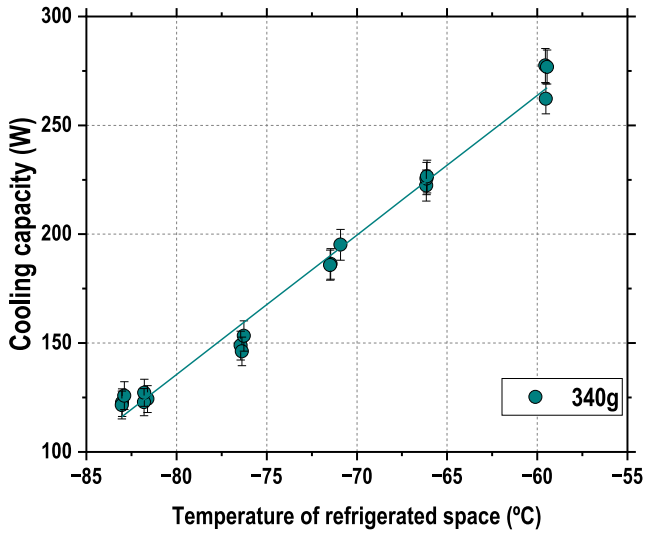

Fig. 13. Cooling capacity vs. temperature of refrigerated space.

'*l*') through the mass balance of the first component with Eq. (A. 6). Following, with the energy and mass balances in the PHS, Eq. (A. 3) to (A. 5), the mass flow rates through the vapour line ($\dot{m}_v$) and through the compressor ($\dot{m}_t$) are determined. Then, using enthalpy calculation at the exit of the evaporator ($h_{o,o}$) and considering isenthalpic lamination at the exit of capillary C1 determines the enthalpy of '*mix*' point. Next, using the temperature measurement at the exit of the CHX of subcooled liquid (point *v,chx,o*) calculates the enthalpy at the inlet of the evaporator (*o,i*) and with the energy balance in the CHX the exit enthalpy of the other current (*chx,o*). Following, using temperature and pressure at suction evaluates the heat transfer rates in the IHX; $\dot{Q}_{v,IHX}$ with Eq.(A. 11), and $\dot{Q}_{l,IHX}$ with Eq.(A. 10); which correspond to the convergence criterion. If the difference of these heat transfer rates is higher than 0.5 W, the mass proportion of the first component is increased, and the routine is executed again.

Finally, when the convergence criteria is satisfied, the enthalpy at the inlet of the evaporator is calculated, assuming an isenthalpic process in capillary C2, to compute the cooling capacity with Eq. (A. 12) and the COP with Eq. (A. 13).

3.2. Method validation

Usually, energy performance calculation validation is made by checking the consistency of heat transfer rates in the heat exchangers; however, in this case, the two energy balances (CHX and IHX) are required to estimate the performance of the system. Since the experimental test rig incorporates additional temperature sensors along the cycle, the consistency of the method is checked by comparing the estimated temperatures of six check points with the values obtained experimentally. Fig. 9 contrasts the estimated temperature values using the calculation method with the measured temperatures in the system. It is corroborated that the model estimates with high accuracy the temperature check points along the cycle. Nearly all temperatures have less than 5 K deviation, although $t_{chx,o}$, has an average deviation of 6.2 K, nonetheless this point is in two-phase condition and the temperature measurement has a large uncertainty. Therefore, the proposed method is consistent and can be used to characterize the AC refrigeration system.

3.3. Uncertainty calculation

The energy performance is calculated using an iterative procedure; thus, uncertainty estimation is made by evaluating the deviation in the results considering the measurement errors of the sensors used (Table 1).

Table A1
Temperature and pressure measurements.

t_{rs} (°C)	t_{env} (°C)	t_{suc} (°C)	t_{dis} (°C)	$t_{k,o}$ (°C)	t_v (°C)	t_l (°C)	$t_{v,chx,o}$ (°C)	$t_{o,i}$ (°C)	$t_{o,o}$ (°C)	$t_{l,sub}$ (°C)	t_{mix} (°C)	$t_{chx,o}$ (°C)	$p_{o,i}$ (bar)	$p_{o,o}$ (bar)	p_{dis} (bar)	p_{phs} (bar)
−83.0	25.3	−22.6	94.2	25.3	25.6	25.8	−54.3	−91.9	−83.5	−6.2	−72.6	−54.3	1.31	1.29	12.05	11.83
−81.7	25.3	−19.9	94.9	25.4	25.6	25.8	−53.1	−91.5	−83.8	−6.4	−71.5	−53.1	1.23	1.22	12.13	11.94
−76.4	25.3	−18.9	94.4	25.4	25.8	26.0	−51.6	−89.2	−82.4	−5.5	−69.0	−51.6	1.32	1.32	12.67	12.45
−71.3	25.3	−10.7	94.5	25.3	25.6	25.8	−48.2	−86.3	−81.3	−4.9	−65.9	−48.2	1.34	1.34	13.35	13.13
−66.1	25.4	−4.2	94.6	25.5	25.9	25.9	−44.0	−85.8	−79.7	−0.9	−62.0	−44.0	1.39	1.39	14.29	14.07
−59.5	25.4	−1.0	94.8	25.4	25.8	25.9	−37.9	−85.1	−76.4	3.4	−56.6	−37.9	1.44	1.44	15.31	15.09

Table A2
Measured and estimated parameters of the operation of the AC system.

t_{rs} (°C)	Z_{tR1150}* (%)	Z_{vR1150}* (%)	Z_{lR1150} (%)	$\dot{m}_t$* (kg/h)	$\dot{m}_l$ (kg/h)	$\dot{m}_v$* (kg/h)	$x_{v_{k,o}}$* (-)	x_{v_l}* (-)	$x_{v_{o,in}}$* (-)	$x_{v_{o,o}}$* (-)	$\dot{Q}_o$* (W)	$\dot{Q}_{CHX}$* (W)	$\dot{Q}_{IHX}$* (W)	P_C (W)	COP* (-)
−83.0	39.7	53.5	21.3	2.38	1.02	1.36	0.68	0.25	0.17	0.34	123.3	689.1	157.4	877.5	0.141
−81.7	40.2	53.8	22.1	2.31	0.99	1.32	0.68	0.26	0.18	0.36	124.8	664.8	157.6	865.9	0.144
−76.4	41.0	55.2	21.9	2.56	1.09	1.46	0.67	0.24	0.19	0.38	149.4	730.9	162.9	905.3	0.165
−71.3	43.2	57.3	22.1	2.76	1.11	1.65	0.69	0.22	0.20	0.42	189.1	811.1	154.7	916.0	0.206
−66.1	45.4	59.4	23.2	2.94	1.14	1.80	0.69	0.21	0.22	0.46	224.8	863.3	146.8	946.3	0.238
−59.5	46.8	61.8	22.8	3.11	1.20	1.91	0.68	0.18	0.26	0.52	272.2	882.5	125.7	981.0	0.277

*Estimated value using the proposed method.

We have extended the method proposed by Moffat [25] as:

The composition of the refrigerant at the point 'l' is evaluated using pressure, temperature, and density with Refprop V.10, as detailed by Eq. (1), so, it has three causes of uncertainty. The uncertainty of this parameter is evaluated as the geometric mean of the deviations caused by each one separately, as detailed by Eq. (2). Each uncertainty is evaluated as the arithmetical mean of the deviation caused by the measurement error of the sensor. For example, in Eq. (3), I_p is the uncertainty associated to the pressure sensor, where Z_{lo} is the calculated composition for the measurement value of the pressure, Z_{lp+} is the composition for the measurement value of pressure plus its measurement error, and Z_{lp-} the composition for the measurement value minus its measurement error. The same is applied to compute the uncertainty caused by temperature, Eq. (4), and that caused by the density, Eq. (5).

$$Z_l = f(p_{phs}, t_{l,sub}, \rho_l) \tag{1}$$

$$I_{Z_l} = \sqrt{I_p^{\,2} + I_t^{\,2} + I_\rho^{\,2}} \tag{2}$$

$$I_p = \frac{|Z_{lp+} - Z_{lo}| + |Z_{lp-} - Z_{lo}|}{2} = \frac{|f(p+\varepsilon_p, t, \rho_l) - Z_{lo}| + |h(p-\varepsilon_p, t, \rho_l) - Z_{lo}|}{2} \tag{3}$$

$$I_t = \frac{|Z_{lt+} - Z_{lo}| + |Z_{lt-} - Z_{lo}|}{2} = \frac{|f(p, t+\varepsilon_t, \rho_l) - Z_{lo}| + |f(p, t-\varepsilon_t, \rho_l) - Z_{lo}|}{2} \tag{4}$$

$$I_\rho = \frac{|Z_{l\rho+} - Z_{lo}| + |Z_{l\rho-} - Z_{lo}|}{2} = \frac{|f(p, t, \rho_l+\varepsilon_\rho) - Z_{lo}| + |f(p, t, \rho_l-\varepsilon_\rho) - Z_{lo}|}{2} \tag{5}$$

This procedure has been extended to all refrigerant compositions (Z_t, Z_l) and to the two representative energy parameters of the system: the cooling capacity and COP. As these cases are estimated using 11 measurement sensors, the method is extended to all of them, as expressed by Eq. (6), where the individual deviations are calculated using Eq. (7). In this equation, X_o is the calculation with the measurement value; X_{j+} the calculated value with the measurement value plus the uncertainty of the device; and X_{j-} the calculated value with the measurement value minus the uncertainty of the device.

$$I_i = \sqrt{\sum_{j=1}^{11} I_j^{\,2}} \tag{6}$$

$$I_j = \frac{|X_{j+} - X_o| + |X_{j-} - X_o|}{2} \tag{7}$$

Fig. 10 depicts the calculated uncertainty using the described method. The method has a percentage uncertainty of mass composition of every stream below 1% over all the tested range, which means that the method can be used to determine the circulating compositions of the fluids with high accuracy. In relation to the energy parameters, it has been calculated that the uncertainty in the cooling capacity is 5.17% at –83.0 °C and is reduced to 2.81% at −59.5 °C. The same happens for the COP, at −83.0 °C the COP uncertainty is of 5.17% and it is reduced as the temperature of the refrigerated space increases up to 2.77% at −59.5 °C.

4. Results

Finally, to complete the work, the results concerning the main operating parameters of the AC cycle over the tested range are included. We do not extend the analysis to refrigerating concepts, since the work focuses on the method proposed to evaluate them.

Fig. 11 presents the calculated mass compositions in quasi-steady-state conditions. It needs to be mentioned that the charging concentration was 0.7 of R-600a and 0.3 of R-1150. It has been calculated that the circulating mass compositions always differ from the charging concentrations, and it is observed that the mass proportion of the most volatile component (R1150) is reduced at lower temperatures, which implies a reduction of the discharge pressure. This agrees with the results of Fig. 6 and also explains the experiments observed in AC systems by other authors [14,15]. In addition, it must be mentioned that the liquid composition nearly remains constant throughout all over the tested range; however, the vapour composition, which provides the cooling effect, reduces the percentage of the most volatile component (R-1150) at low temperatures, thus reducing the potential of the AC system to work at lower temperatures. In fact, for the considered test, it was not possible to reduce the temperature of the refrigerated space any further.

Finally, Fig. 12 represents the COP value and its uncertainty, and Fig. 13 the provided cooling capacity and its uncertainty. They present a trend in agreement with the performance of refrigeration systems, that is

that both parameters decrease when the temperature of the refrigerated space does. It needs to be mentioned that, to the knowledge of the authors, this is the first time that the COP and cooling capacity of an AC refrigeration system has been measured. The estimated uncertainties are acceptable and inside the range usually accepted in refrigeration systems. To reduce the uncertainty a possibility would be including additional Coriolis mass flow meters, which would be difficult without modifying the normal behaviour of the cycle.

5. Conclusions

This work focuses on the thermodynamic evaluation of a single stage AC refrigeration system working with a mixture of R-600a/R-1150 with a charging composition of 70/30%. For the first time, this work describes an experimental procedure that allows for the calculation of the circulating compositions of the system as well as its energy performance parameters.

Using an instrumented experimental test rig and an experimental test that covers temperatures of the refrigerated space from −59.5 to −83.0 °C at a constant temperature of the climatic chamber, this work establishes a new methodology to evaluate the operating parameters of the system. The proposed method is based on a liquid density measurement in the system and a convergence criterion based on the heat balance in the two main heat exchangers, the cascade heat exchanger and the internal heat exchanger or recuperator. The method uses only 11 sensor measurements, and it is able to characterize the rest of thermodynamic states of the fluid in the cycle. The method has been validated using 6 additional temperature measurements in the test, showing an agreement with errors below 5 K in most points. Additionally, the uncertainty calculation of the compositions indicates that the method can estimate the main compositions with an uncertainty below 1%, the cooling capacity below 5.17% and the COP below 5.17%. It has been concluded that the uncertainty increases as the temperature of the refrigerated space is reduced.

Additionally, the calculation method has revealed a large discrepancy between the mass charging composition and that during the operation of the plant, which also varies as the temperature of the refrigerated space changes. The obtained tendencies of the circulating composition explain the quasi-steady-state behaviour of the plant and agree with the few published works about AC refrigeration systems.

Finally, the method allowed for the calculation of the COP of the AC system, which ranges from 0.140 ± 5.2% at −83.0 °C to 0.277 ± 2.8% at −59.5 °C for an environment temperature of 25.0 ± 0.5 °C. It needs to be mentioned that the AC system was not energy optimized, therefore these values are only indicative.

Declaration of Competing Interest

The authors declare that they have no known competing financial interests or personal relationships that could have appeared to influence the work reported in this paper: [Rodrigo Llopis reports financial support was provided by Spain Ministry of Science and Innovation. Rodrigo Llopis reports financial support was provided by Generalitat Valenciana Presidencia.].

Data availability

Experimental data used for the work is included in the manuscript for use by other researchers.

Acknowledgements

Grant TED2021-130162B-I00 funded by MCIN/AEI/ 10.13039/501100011033 and by "ERDF A way of making Europe" by the "European Union". Grant CIAEST/2021/14 funded by the Generalitat Valenciana.

Authors want to acknowledge the company Frost-Trol S.A. (www.frost-trol.com) for the implication in the project and by manufacturing the used refrigerated space, and to Gabriele Toffoletti and Emanuele Sicco during the set-up of the plant.

Appendix 1. Equations used to determine the energy performance.

This annex details the equations, based on steady-state regime, used to characterize the auto-cascade system.

Thermodynamic properties

The thermodynamic properties are evaluated using Refprop v.10 database [23] with the standard mixing coefficients for the mixture R-600a/R-1150 ($\beta_T = 0.99502$, $\gamma_T = 1.057$, $\beta_v = 1.0$, and $\gamma_v = 1.0$). According to Eq. (A. 1), calculation of each thermophysical property requires two input properties (p, t, h, x,…) and the corresponding mass composition (Z).

$$(h,\ \rho, x,\ t, \ldots) = f(\text{'}Property\ 1\text{'}, \text{'}Property 2\text{'}, Z) \tag{A1}$$

Phase separator

Fractionation in the phase separator is calculated using Bell & Deiters [24] correlations developed for closed systems. The corresponding rules of fractionation are available in Refprop, thus, mass compositions of saturated liquid and vapour in equilibrium are only function of the vessel pressure and the composition of the inlet current of fluid (Z).

$$[Z_{l,e}, Z_{v,e}] = f(p_i, Z) \tag{A2}$$

Mass balance:

$$\dot{m}_t = \dot{m}_l + \dot{m}_v \tag{A3}$$

Mass balance of the first component of the mixture, where $Z_v = Z_{v,e}$:

$$\dot{m}_t \cdot Z_t|_1 = \dot{m}_l \cdot Z_l|_1 + \dot{m}_v \cdot Z_v|_1 \tag{A4}$$

Energy balance:

$$\dot{m}_t \cdot h_{k,o} = \dot{m}_l \cdot h_l + \dot{m}_v \cdot h_v \tag{A5}$$

Vapour title at the liquid exit, where Z_l is the liquid composition determined with the density value of the Coriolis mass flow meter, pressure and temperature at *l,sub* point.

$$x_l = \frac{Z_l - Z_{l,e}}{Z_{v,e} - Z_{l,e}} \tag{A6}$$

Mixing point

Energy balance:

$$\dot{m}_t \cdot h_{mix} = \dot{m}_v \cdot h_{o,o} + \dot{m}_l \cdot h_{l,exp,o} \tag{A7}$$

Cascade heat exchanger

Heat transfer through the line with more proportion of most volatile component:

$$\dot{Q}_{v,CHX} = \dot{m}_v \cdot \left(h_v - h_{v,chx,o}\right) \tag{A8}$$

Heat transfer through the line with less proportion of most volatile component:

$$\dot{Q}_{l,CHX} = \dot{m}_t \cdot \left(h_{chx,o} - h_{mix}\right) \tag{A9}$$

Internal heat exchanger

Heat transfer through the line with less proportion of volatile component:

(A10). $\dot{Q}_{l,IHX} = \dot{m}_l \cdot (h_l - h_{l,sub})$

Heat transfer through the line going to compressor suction:

(A11). $\dot{Q}_{v,IHX} = \dot{m}_t \cdot (h_{suc} - h_{CHX,o})$

Refrigerated space

Cooling capacity:

(A12). $\dot{Q}_o = \dot{m}_v \cdot (h_{o,o} - h_{o,i})$

Auto-cascade system

Energy efficiency or Coefficient of Performance:

(A20). $COP = \frac{\dot{Q}_o}{P_C}$

The temperature of the refrigerated space is calculated as mean of 4 t-type thermocouples.

Appendix 2. Experimental data of the auto-cascade system for R600a/R1150 [70/30%$_{mass}$] at $t_{env} = 25$ °C

This annex details the measured data and estimated data (*) using the proposed method of the auto-cascade refrigeration system. Each value corresponds to the average of three steady-state test conditions registered at the end of the compressor cycling process.

References

[1] International Institute of Refrigeration, UNEP, Cold chain technology Brief: Vaccines, in, 2021.

[2] A. Mota-Babiloni, M. Mastani Joybari, J. Navarro-Esbrí, C. Mateu-Royo, Á. Barragán-Cervera, M. Amat-Albuixech, F. Molés, Ultralow-temperature refrigeration systems: configurations and refrigerants to reduce the environmental impact, Int. J. Refrig. 111 (2020) 147–158.

[3] European Commission, Regulation (EU) No 517/2014 of the European Parliament and of the Council of 16 April 2014 on fluorinated greenhouse gases and repealing Regulation (EC) No 842/2006., (2014).

[4] Q. Wang, D.H. Li, J.P. Wang, T.F. Sun, X.H. Han, G.M. Chen, Numerical investigations on the performance of a single-stage auto-cascade refrigerator operating with two vapor–liquid separators and environmentally benign binary refrigerants, Appl. Energy 112 (2013) 949–955.

[5] Y. He, H. Wu, Y. Liu, T. Wang, X. Wu, C. Cheng, T. Jin, Theoretical performance comparison for two-stage auto-cascade refrigeration system using hydrocarbon refrigerants, Int. J. Refrig. (2022).

[6] G. Yan, J. Chen, J. Yu, Energy and exergy analysis of a new ejector enhanced auto-cascade refrigeration cycle, Energ. Conver. Manage. 105 (2015) 509–517.

[7] G. Yan, H. Hu, J. Yu, Performance evaluation on an internal auto-cascade refrigeration cycle with mixture refrigerant R290/R600a, Appl. Therm. Eng. 75 (2015) 994–1000.

[8] E.Á. Rodríguez-Jara, F.J. Sánchez-de-la-Flor, J.A. Expósito-Carrillo, J.M. Salmerón-Lissén, Thermodynamic analysis of auto-cascade refrigeration cycles, with and without ejector, for ultra low temperature freezing using a mixture of refrigerants R600a and R1150, Appl. Therm. Eng. 200 (2022), 117598.
[9] J. Liu, Y. Liu, G. Yan, J. Yu, Theoretical study on a modified single-stage autocascade refrigeration cycle with auxiliary phase separator, Int. J. Refrig 122 (2021) 181–191.
[10] J. Liu, Y. Liu, G. Yan, J. Yu, Thermodynamic analysis on a modified auto-cascade refrigeration cycle with a self-recuperator, Int. J. Refrig 137 (2022) 117–128.
[11] D. Li, T. Bai, J. Yu, Thermodynamic performance optimization and analysis of an auto-cascade refrigeration cycle with vapor injection for ultra-low temperature freezer, Int. J. Refrig 145 (2023) 425–435.
[12] Y. He, H. Wu, K. Xu, Y. Zhang, T. Wang, X. Wu, C. Cheng, T. Jin, Theoretical performance comparison for a regenerator-enhanced three-stage auto-cascade refrigeration system using different zeotropic mixed refrigerants, Energ. Buildings 283 (2023), 112815.
[13] J. Chen, Z. Zhang, D. Wang, G. Wang, X. Peng, X. Qin, H. Li, Comparative study on four autocascade refrigeration cycles based on energy, exergy, economic and environmental (4E) analyses, Energ. Conver. Manage. 288 (2023), 117129.
[14] C. Aprea, A. Maiorino, Autocascade refrigeration system: experimental results in achieving ultra low temperature, Int. J. Energy Res. 33 (2009) 565–575.
[15] K. Du, S. Zhang, W. Xu, X. Niu, A study on the cycle characteristics of an auto-cascade refrigeration system, Exp. Therm Fluid Sci. 33 (2009) 240–245.
[16] L. Zhang, S. Xu, P. Du, H. Liu, Experimental and theoretical investigation on the performance of CO2/propane auto-cascade refrigerator with a fractionation heat exchanger, Appl. Therm. Eng. 87 (2015) 669–677.
[17] T. Bai, G. Yan, J. Yu, Experimental investigation of an ejector-enhanced auto-cascade refrigeration system, Appl. Thermal Eng. 129 (2018) 792–801.
[18] T. Bai, G. Yan, J. Yu, Experimental research on the pull-down performance of an ejector enhanced auto-cascade refrigeration system for low-temperature freezer, Energy 157 (2018) 647–657.
[19] Y. Qin, N. Li, H. Zhang, B. Jin, B. Liu, Experimental characterization of an innovative refrigeration system coupled with Linde-Hampson cycle and auto-cascade cycle for multi-stage refrigeration temperature applications, Energy 240 (2022), 122498.
[20] Z. Liu, M. Bai, H. Tan, Y. Ling, Z. Cao, Experimental test on the performance of a −80 °C cascade refrigeration unit using refrigerants R290–R170 for COVID-19 vaccines storage, J. Build. Eng. (2022), 105537.
[21] B. Sreenivas, H.G. Nayak, G. Venkatarathnam, Relationship between composition of mixture charged and that in circulation in an auto refrigerant cascade and a J-T refrigerator operating in liquid refrigerant supply mode, Cryogenics 81 (2017) 42–46.
[22] Q. Chen, Y. Li, Experimental Investigation on intermittent operation characteristics of dual-temperature refrigeration system using hydrocarbon mixture, Energies 15 (2022).
[23] Lemmon E. W., B. I.H., H.M. L., M.M. O., NIST Standard Reference Database 23: Reference Fluid Thermodynamic and Transport Properties-REFPROP, Version 10.0, National Institute of Standards and Technology, (2018).
[24] I.H. Bell, U.K. Deiters, On the construction of binary mixture p-x and T-x diagrams from isochoric thermodynamics, AIChE J. 64 (2018) 2745–2757.
[25] R.J. Moffat, Using uncertainty analysis in the planning of an experiment, J. Fluids Eng. 107 (1985) 173–178.